3-1994

Slowing of ^{85}Rb Atoms with Isotropic Light

Herman Batelaan
University of Nebraska - Lincoln, hbatelaan@unl.edu

S. Padua
SUNY Stony Brook

D. H. Yang
Peking University

C. Xie
SUNY Stony Brook

R. Gupta
SUNY Stony Brook

See next page for additional authors

PHYSICAL REVIEW A VOLUME 49, NUMBER 4 APRIL 1994

Slowing of ^{85}Rb atoms with isotropic light

H. Batelaan, S. Padua, D. H. Yang,* C. Xie, R. Gupta, and H. Metcalf
Physics Department, State University at Stony Brook, Stony Brook, New York 11790
(Received 25 August 1993)

We have demonstrated the slowing of a rubidium atomic beam by isotropic monochromatic light. The results agree with a model calculation, thus allowing its use for designing a practical isotropic light slower. The large hyperfine splittings of rubidium lead to natural multifrequency slowing, which is also included in our model.

PACS number(s): 32.80.Pj, 42.50.Vk

I. INTRODUCTION

The ultimate goal for atomic-beam slowing and cooling is the compression of the entire velocity distribution of atoms in a beam as they emanate from a source to one narrow peak at a desired low velocity. Although this goal is far from being reached at present, atomic-beam slowers are commonly used for atomic clocks and for loading of magneto-optical traps and optical molasses. Improvements to atomic-beam slowers are therefore of current interest. Recently slowing and cooling by white light [1] and isotropic monochromatic light [2] have been demonstrated to be promising new techniques.

In isotropic laser light, the resonance frequency ω_{if} of an atom moving at a velocity v will be matched by the Doppler-shifted laser frequency when the wave vector $\vec{k}$ of the light makes an angle θ with the atomic velocity $\vec{v}$:

$$\omega_{if} = \omega_l - kv\cos\theta, \tag{1}$$

where ω_l is the laser frequency and i (f) indicates the initial (final) state. For red detuned light ($\omega_l - \omega_{if} < 0$) this resonance condition requires $\theta > \pi/2$, meaning that the recoil caused by the absorbed photons opposes the atomic motion and slows the atoms. Subsequent spontaneous emission does not exert a force on the atoms on average. As the atoms are decelerated, they absorb light from a increasing angle θ (angle tuned), until the maximum value of θ ($= \pi$) is reached. Because the light is isotropic, the atomic motion is directly opposed irrespective of its direction, while for slowing with a directed laser beam using Zeeman (magnetically tuned) [3] and chirped (frequency tuned) [4] compensation, only the longitudinal velocity component of the atomic motion is opposed. This major advantage prevents the atomic beam from being transversely expanded (apart from spontaneous emissions), in contrast to Zeeman tuned and chirped slowing.

In this article, we describe the application of the isotropic light slowing technique to a rubidium beam in order to test experimental techniques and a numerical model for the slowing process. The resulting slowed beam of cold atoms is enhanced by natural multifrequency slowing [2], for which the rubidium atom has an appropriate hyperfine splitting of the excited state. The carefully tested model is then used to calculate isotropic slowing over an extended length.

II. EXPERIMENT

A schematic view of our apparatus is shown in Fig. 1. A thermal beam of Rb is collimated to ~10 mrad by an aperture (A1) suspended from a cold trap and travels through a slower made from the diffusely reflective material Spectralon [5]. The 20 cm long cylindrical slower has an inner diameter of 3 mm and outer diameter of 2 cm. The reflectivity r of the material is specified by the

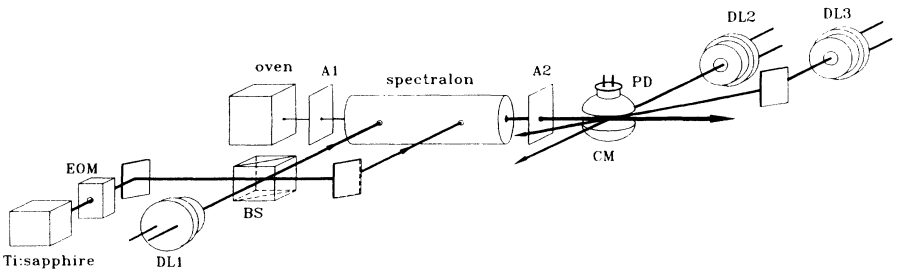

FIG. 1. A schematic view of the apparatus. An explanation of its components is given in the text.

*Permanent address: Peking University, Beijing, China.

manufacturer to be 99.1%. A beam from a Ti:sapphire laser, split into two branches by a beam splitter (BS), enters the tube via two 1 mm diameter holes situated 5 cm from each cylinder end. The laser light has a line width of $\leq$ 1 MHz and is side locked to the Doppler broadened $5S_{1/2} \rightarrow 5P_{3/2}$ transition of Rb near $\lambda = 780$ nm with an accuracy of $\pm$ 50 MHz using absorption in a vapor cell. Saturated absorption is used to calibrate the Doppler broadened absorption spectrum frequency scale. An electro-optical modulator (EOM) [6] divides the laser power between the main laser frequency $\omega_l = 2\pi\nu_1$ (Fig. 2) and two sidebands at $\omega_l \pm (2\pi \times 2.91$ GHz). One sideband (ν_2) counteracts optical pumping into a single ground state hyperfine sublevel, while the other is not used. Alternatively, we use the Ti:sapphire laser and a Sharp model LTO25 diode laser (DL1) to provide two frequencies, instead of the EOM.

The laser beam from another Sharp model LTO24 diode laser (DL3) is directed at an angle of 30° with the atomic beam and intersects it downstream from the end of the Spectralon tube. This is used to the determine the longitudinal velocity distribution by measuring the intensity of the emitted fluorescence as a function of the laser frequency. The saturated absorption signal from this laser also serves as a calibration of its frequency. A beam from a frequency locked laser (DL2) perpendicular to the atomic beam cancels velocity selective optical pumping effects.

Two concave spherical mirrors (CM) collect the fluorescence [7,8] and focus it on a hybrid photodiode-amplifier detector (PD) [9]. Stray laser light emanating from the Spectralon tube is shielded from the detector (aperture A2). We chop the side bands of the EOM at 500 Hz and subtract the gated signal from the gated background to reduce the noise markedly. This also means that below an atomic velocity of 100 m/s the gated detection affects the signal.

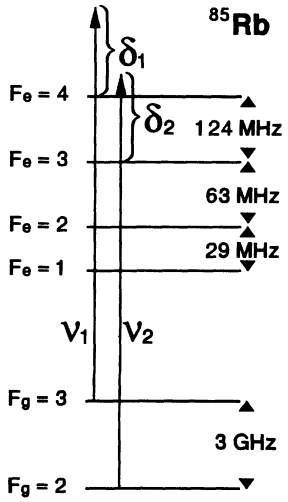

FIG. 2. A scheme of the relevant energy levels of ^{85}Rb.

III. A MODEL CALCULATION

We assume that the initial longitudinal velocity distribution of the atomic beam is thermal and given by [10]

$$f(v) \propto v^3 e^{-mv^2/2k_BT}, \tag{2}$$

where k_B is the Boltzman constant and T is the oven temperature. The force on the atoms can be written as

$$F(z) = \int \sum_{g,e} (\Pi_g R_{ge} c_{ge} p - \Pi_e R_{eg} c_{eg} p) d\Omega, \tag{3}$$

where the subscript $g(e)$ indicates the ground (excited) hyperfine levels, Π indicates the steady state population, and Ω $[=(\theta,\phi)]$ indicates the direction from which an atom absorbs light. The angle θ is defined relative to the direction of the atomic motion. The projection of the recoil momentum of the atom p along its direction of motion is given by

$$p = \hbar k \cos\theta. \tag{4}$$

The transition rate [11] from an initial (i) state to a final (f) state is determined by

$$c_{if} = (2J_i + 1)(2F_f + 1) \left\{ \begin{matrix} F_f & 1 & F_i \\ J_i & I & J_f \end{matrix} \right\}^2 \frac{1}{\tau}. \tag{5}$$

Here the initial (final) state can be either the ground or excited state. The lifetime τ of the excited J_e state (for the $5\,^2P_{3/2}$ state of ^{85}Rb) is 27 ns [12]; $I = 5/2; J_g = 1/2; J_e = 3/2; F_g = 2,3; F_e = 1,2,3,4$; and $\{\ \}$ are the usual 6-j symbols [13]. The photon scattering rate $R_{if}(z,v)$ is proportional to the convolution of the laser frequency distribution I inside the tube and the atomic line shape $S_{if}(\omega)$ associated with the transition from the initial to the final state [14]

$$R_{if}(z,v) = \frac{\Gamma c \lambda^2}{8\pi} \rho(z) \int \int_0^\infty \frac{S_{if}(\omega) I_{if}(v,\omega,\theta)}{\hbar\omega} d\omega\, d\Omega, \tag{6}$$

where $\Gamma = 1/\tau$ ($= 2\pi \times 6$ MHz) is the atomic linewidth for ^{85}Rb and $\rho(z)$ is the light energy density at position z. In the atomic line shape

$$S_{if}(\omega) = \frac{\Gamma/\pi}{(\omega - \omega_{if})^2 + \Gamma^2} \tag{7}$$

$\omega_{if} = \omega_f - \omega_i$ denotes the frequency difference between the hyperfine levels F_f and F_i. Here I is the normalized laser frequency distribution in the atomic rest frame

$$I_{if}(v,\omega,\theta) = \frac{1}{4\pi^2} \frac{\Gamma_l}{(\omega - \omega_l + kv\cos\theta)^2 + \Gamma_l^2} d\Omega, \tag{8}$$

where Γ_l is the laser linewidth.

The energy density $\rho(z)$ is derived by an iterative procedure [15]. For a Lambertian reflector, which obeys

$$J(\alpha) = J_0 \cos\alpha, \tag{9}$$

where J_0 is the incident laser power and $J(\alpha)$ the reflected power at an angle α with respect to the normal of the reflector surface, a straightforward derivation for a cylindrical geometry yields

$$P_n(z) = r^n \int_0^L \int_0^{2\pi} \left(\frac{r_c(1-\cos\phi)}{(z'-z)^2 + 2r_c^2(1-\cos\phi)} \right)^2 \times P_{n-1}(z') r \, d\phi \, dz', \quad n = 1, 2, \ldots \quad (10)$$

for the power distribution P_n of the nth reflection of the laser light in the cylinder. The initial power distribution is given by P_0. For example, with one entrance hole at $z = 0$ the total laser power $P = P_0(0)$ and $P_0(z \neq 0) = 0$. The length of the cylinder is L, the radius r_c and the reflectivity r. We have assumed that the power distribution is symmetric in ϕ. The total power distribution may be obtained by summing over all reflections, $P(z) = \sum_{n=0}^{\infty} P_n(z)$. We can immediately calculate the energy density from [10]

$$\rho(z) = 4P(z)/c \quad (11)$$

by assuming that the power distribution is isotropic. We have verified analytically that for an infinite cylinder, for which the surface is a homogeneous, Lambertian source the power distribution is isotropic. These approximations are motivated by the small radius over length ratio for the cylinder.

In the force expression the steady state populations Π_e, Π_g of the hyperfine levels as a function of the position z are calculated by substituting $R_{if}(z, v)$ in the rate equations [11,16]. Obtaining from the calculated force the final velocity of the atom v_f for each initial velocity v_i, we obtain the final velocity distribution

$$f(v_f) = \frac{dv_i}{dv_f} f(v_i), \quad (12)$$

expressing the conservation of atoms.

IV. RESULTS

To test the effective laser power in the tube we measured and calculated the fraction of atoms optically pumped from the F_g=3 into the F_g=2 state as a function of laser power injected into the Spectralon tube. We chose this fraction to be the ratio of the maxima of the atomic velocity distribution with and without laser power, and plotted the result in Fig. 3. The calculation is the result of the time dependent rate equations [16] with the isotropic photon scattering rate [Eq. (6)] for r=99%.

For an oven temperature of $T = 130°$ C the density of rubidium results in an estimated mean free path for photons of 6 cm, while for an oven temperature of T= 170 ° C the mean free path is only 0.6 cm. On the other hand, photons travel on average 2.5 cm before being absorbed by a tube with a 92% reflectivity (see below) and 3 mm diameter. Therefore we attribute the decrease in the optical pumping efficiency with increasing temperature to the optical thickness of the atomic beam and

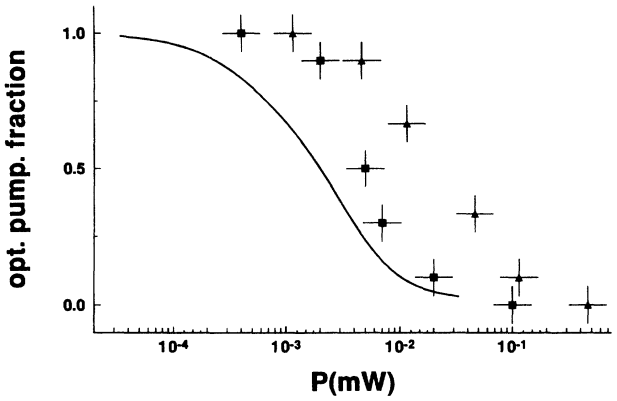

FIG. 3. Fraction of atoms in the F_g=3 state after the atoms pass through the slower for oven temperatures of 170° (▲) and 130° (■) is given. The line is the calculated result from the rate equations for a 99% reflectivity.

to strongly Doppler-shifted fluorescence from all these atoms that is prevented from escaping by multiple reflections in the tube. All velocity distributions presented below were taken with an oven temperature of $T = 130$ ° C where the atomic beam is not optically thick. The optical pumping efficiency test is thus used as an atomic calibration of the energy density inside the Spectralon tube.

Still, roughly a factor of 4 discrepancy exists between the measured and the calculated optical pumping efficiency. An additional experimental test revealed the source of the problem. Figure 4 shows the result of a measurement of the relative light power that has diffused to the outside of the tube as a function of position along it. The experimental result for a Rb-exposed Spectralon tube before and after cleaning were compared with the result calculated from Eq. (10). The results for the relative light power were scaled appropriately. The drop in

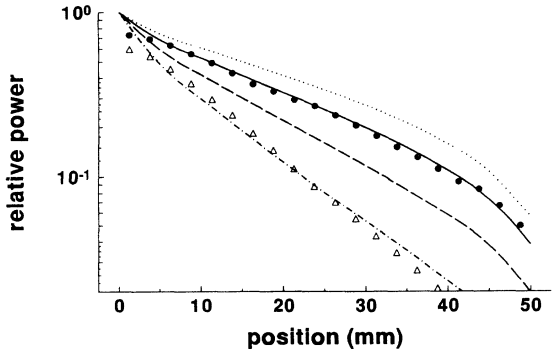

FIG. 4. Laser power measured as a function of position along the external wall of the Rb-exposed Spectralon tube of 10 cm length before (△) and after (•) cleaning. The calculated power is given for r =99% (···), 98% (—), 96% (– – –), and 92% (– · – · –). The results are scaled appropriately. The laser beam enters the tube at the zero position.

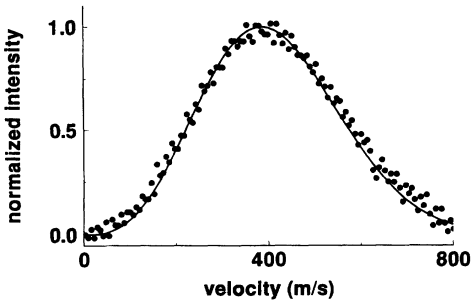

FIG. 5. The measured and calculated initial velocity distribution.

reflectivity of the exposed tube corresponds to a factor of 4 drop in intensity. In accordance with the atomic calibration of the energy density, we used a factor 4 to correct the laser power in all subsequent calculations for the velocity distributions. The contamination of the surface of the Spectralon tube could possible be reduced by a carefully placed cold trap.

The measured fluorescence spectrum was used to determine the velocity distribution, which has contributions from each of the three accessible excited hyperfine states. A given frequency of the detection laser corresponds to three different detunings, which in their turn via $\delta_{if} = kv_{if}\cos\theta$ correspond to atoms with three different longitudinal velocities. In our case, the repumping detection laser (DL2) was strongly saturating, while the frequency ramped detection laser (DL3) was operated in the linear range, causing the relative strengths of the different contributions to be proportional to c_{if}. Taking these three corrections into account in our calculated distributions gives excellent agreement with the experimental result for the initial velocity distribution (Fig. 5).

In Fig. 6 the difference between the final and initial velocity distribution is shown. A negative value of this difference indicates that atoms have been removed, while a positive value shows an increase in the number of atoms. Figure 6(a) shows that atoms around 400 m/s have been slowed to velocities around 150 m/s. The experimental detuning δ_1 (Fig. 2) is -190 ± 50 MHz relative to the F_g=3 to F_e=4 transition and the detuning used in the calculation is -210 MHz. The EOM is driven at 2.91 $\pm$ 0.01 GHz, which means that the detuning δ_2 relative to the F_g=2 to F_e=3 transition is also -190 MHz. The total laser power $P = 100$ mW and the ratio β of each EOM sideband over carrier is $\beta = 1$. The vertical scale is normalized to the height of the maximum of the initial atomic velocity distribution, so that the peak of slowed atoms [Fig. 6(a)] contains ~2% of all the incident atoms.

The acceleration in the velocity distribution shown in Fig. 6(b) has been measured under the same experimental conditions as in Fig. 6(a), except for a positive 190 MHz detuning. The presence of the double dip structure can be mostly attributed to the F_g=3 to F_e=4 and to the F_g=3 to F_e=3 transitions. The Doppler resonance condition [Eq. (1)] is met for the F_g=3 to F_e=4 transition at 170 m/s and for the F_g=3 to F_e=3 transition at 280 m/s, which agree with the positions of the dips.

For negative detuning the Doppler resonance condition [Eq. (1)] is met for the F_g=3 to F_e=4 transition at 170 m/s and for the F_g=3 to F_e=3 transition at 60 m/s. Since the interaction time is longer at low velocities, the slowing process is more efficient than the acceleration process, and the two peaks merge into one. This is natural multifrequency slowing and is especially effective because of the appropriate hyperfine splitting of Rb. It cannot be exploited in sodium [2], where the hyperfine splitting is too small. Instead one must assist the angle-tuned slowing with a stepwise change in laser frequency (multifrequency slowing). The large excited state hyperfine splitting of rubidium provides this effect naturally.

The results in Figs. 6(c) and 6(d) have been measured for a ratio of EOM sideband over carrier $\beta = 0.02$. For positive detuning the resonance condition (at 170 m/s) can only be met by the cyclic F_g=3 to F_e=4 transition. Therefore a weak repumping sideband is sufficient to maintain the acceleration process. However, for negative detuning the F_g=3 to F_e=3 (and F_g=3 to F_e=2)

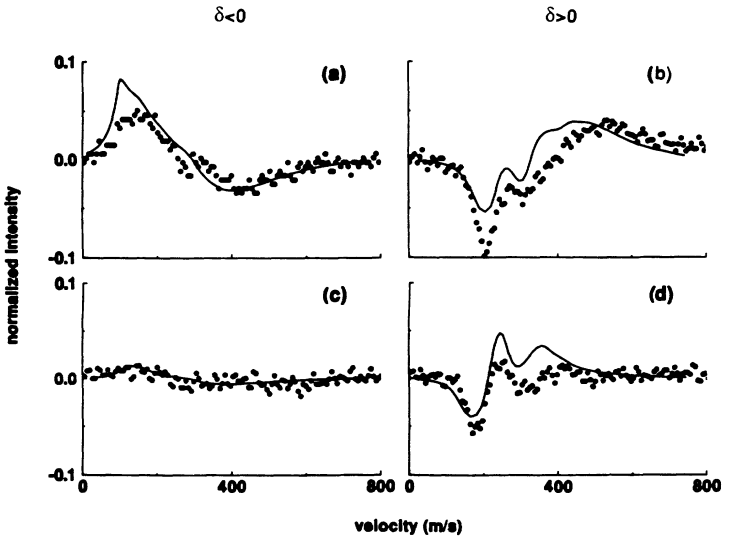

FIG. 6. The difference between the slowed and initial atomic velocity distribution. The experimental and calculated results show agreement. The total laser power is $P = 100$ mW. (a) Natural multifrequency slowing, $\delta = -190 \pm 50$ MHz, $\beta = 1$. (b) Acceleration showing two dips, $\delta = 190 \pm 50$ MHz, $\beta = 1$. (c) Slowing disappears, $\delta = -190 \pm 50$ MHz, $\beta = 0.02$. (d) Acceleration remains, $\delta = 190 \pm 50$ MHz, $\beta = 0.02$.

transition can excite atoms at 170 m/s due to angle tuning. This means that a weak repumping sideband is not sufficient to maintain the slowing process.

Finally, having established confidence in the numerical model by the agreement with the measurements, we show the result of calculations for a 20, 60, and 100 cm long slower with a 500 mW input power (Fig. 7). In analogy with the usual definition for the saturation parameter $s = 2\Omega^2/\Gamma^2$, where Ω is the Rabi frequency, we define $s = 2(c_{ge}R_{ge})^2/\Gamma^2$. For the 100 cm slower a 500 mW input, this amounts to $s = 12.5$ at the position where the laser light enters the slower for atoms moving at a 100 m/s velocity. At the end of the tube $s < 1$. For the 20 cm slower the atoms are saturated throughout the slower. This explains why the slowed peak increases with increased length of the slower. Below saturation this does not occur. We also point out that the broad slowed peak for the 20 cm slower has been compressed by the natural multifrequency slowing for the 100 cm slower. Note that the fraction of atoms around 50 m/s has increased by a factor of 100 over the initial distribution. Because this strong increase shows promise for important applications of this technique, we are currently building an extended length slower.

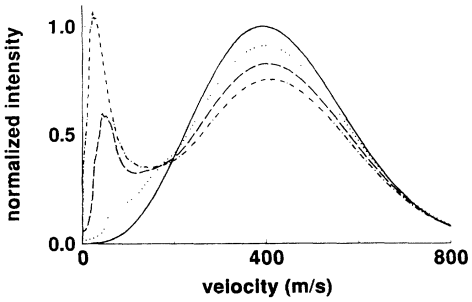

FIG. 7. Calculated initial (solid line) and final atomic velocity distributions for $\delta = -75$ MHz, $P = 500$ mW, r=92%, $\beta = 0.5$, and the EOM is driven at 2.97 GHz. The lengths of the slower are 20 cm ($\cdots$), 60 cm ($- - -$), and 100 cm ($- \cdot - \cdot -$). The largest slowed peak at 50 m/s contains ~25% of all incident atoms.

ACKNOWLEDGMENTS

We thank Alex Martin, Wolfgang Ketterle, and Edgar Vredenbregt for helpful discussions. This work was supported by NSF, ONR, AFOSR, and CAPES (Brazil).

[1] M. Zhu, C. W. Oates, and J. L. Hall, Phys. Rev. Lett. **67**, 46 (1991).
[2] W. Ketterle, A. Martin, M. A. Joffe, and D. E. Pritchard, Phys. Rev. Lett. **69**, 2483 (1992).
[3] W. D. Phillips, J. V. Prodan, and H. J. Metcalf, J. Opt. Soc. Am. B **2**, 1755 (1985).
[4] W. Ertmer, R. Blatt, J. L. Hall, and M. Zhu, Phys. Rev. Lett. **54**, 996 (1985).
[5] Labsphere Inc., P. O. Box 70, North Sutton, NH 03260.
[6] We thank New Focus Corp. (340 Pioneer Way Mountain View, CA 94041) for loaning us the electro-optic modulator.
[7] K. Shimizu and F. Shimizu, J. Chem. Phys. **78**, 1126 (1983).
[8] U. Hefter and K. Bergmann, in *Atomic and Molecular Beam Methods*, edited by Giacinto Scoles (Oxford University Press, New York, 1988).
[9] United Detector Technology, 12525 Chadron Avenue, Hawthorne, CA 90250.
[10] F. Reif, *Fundamentals of Statistical and Thermal Physics* (McGraw-Hill, New York, 1965).
[11] E. de Clercq, M. de Labachellerie, G. Avila, and M. Tetu, J. Phys. (Paris) **45**, 239 (1984).
[12] C. E. Theodosieu, Phys. Rev. A **30**, 2899 (1984).
[13] M. Rotenberg, R. Bivins, N. Metropolis, and J. K. Wooten, *The 3J and 6J Symbols* (Crosby Lockwood, London, 1959).
[14] P. W. Milonni and J. H. Eberly, *Lasers* (Wiley, New York, 1988), pp. 220–227.
[15] For the case of a sphere, see D. G. Goebel, Appl. Opt. **6**, 125 (1967).
[16] G. Avila, V. Giordano, V. Candelier, E. de Clercq, G. Theobald, and P. Cerez, Phys. Rev. A **36**, 3719 (1987).